NUCL SCI TECH (2018) 29:119
https://doi.org/10.1007/s41365-018-0455-4

Design of a shielding collimator device for a small-angle monoenergetic neutron source

Wen-Hui Lü[1,2] · Hui-Ping Guo[1] · Ning Lü[1] · Kuo Zhao[1] · Xiao-Tian Wang[1] · Yi-Jie Hou[1]

Received: 30 August 2017 / Revised: 5 February 2018 / Accepted: 28 February 2018 / Published online: 5 July 2018

Abstract To obtain a small-angle monoenergetic neutron source, a shielding collimator device is designed for the neutron source generated by a neutron tube. The device is divided into the collimator and the capture cave. The collimator is made of three layers of stainless steel and borated polyethylene and is used to constrain neutrons in a small angle. The capture cave is used to increase the number of times neutron inelastic scattering occurs in the opposite direction of the radiation field, thereby reducing the proportion of scattered neutrons in the radiation field. Material thickness, aperture size, and the optimum structure of the capture cave were simulated using MCNP. The design features a neutron emission angle within a range of 3° and neutron fluxes in the radiation field, which are higher by two orders of magnitude than those outside the radiation field. This research has practical value for the generation of monoenergetic small-angle neutron sources and neutron applications.

Keywords Neutron tube · Monte Carlo simulation · Collimation · Shield

We wish to thank Professor Hua-Si Hu of Xi'an Jiao Tong University for his help. He gave us good suggestions throughout this project.

✉ Wen-Hui Lü
lvmh14@mails.tsinghua.edu.cn

1 Xi'an Research Institute of Hi-Tech, Xi'an 710025, China

2 Key Laboratory of Particle and Radiation Imaging (Ministry of Education) and Department of Engineering Physics, Tsinghua University, Beijing 100083, China

1 Introduction

Neutron sources are essential in numerous fields of studies, and their applications include neutron dosimeter validation tests, neutron radiography techniques, studies on neutron radiation characteristics in new materials, and research on radiation hardening techniques [1, 2]. Commonly used neutron sources include the isotopic source and the small-sized neutron generator [3]. Isotopic sources, such as Am–Be, Am–B, and ^{252}Cf exhibit energy spread, which causes energy response errors in the detection and application of neutrons. Hence, small-sized neutron generators, such as D–D and D–T tubes, play an irreplaceable role as monoenergetic neutron sources in neutron applications [4].

The advantages of neutron tubes are the monoenergetic neutrons produced by neutron tubes, high neutron yield, and the fact that neutron tubes do not produce radiation when they are not operating, making them convenient for management, storage, and transportation. However, drawbacks still exist for the neuron source generated by the neutron tube. First, the exit direction of the neutrons is approximately isotropic, which is unsuitable for small-angle neutron source application. Second, neutron scattering makes neutrons less monoenergetic [5].

To obtain a small-angle monoenergetic neutron source using neutron tubes, a shielding collimator device is designed based on the neutrons generated by D–D and D–T neutron tubes. Neutrons generated by a D–D tube have relatively low levels of energy and can be collimated and shielded easily. Therefore, high-energy (14.1 MeV) neutrons generated by a D–T neutron tube are selected as the research subject.

2 Design concept

2.1 Problem description

Neutron scattering influences the neutron radiation field, which can usually be estimated using the shadow cone method. The shadow cone method involves placing a shielding material between the radiation source and the detector. The radiation recorded by the detector comes from the scattering. The shielding material should be thick enough to ensure that the detector will not be affected by the source. However, when the detector and neutron source are relatively close, the energy response of the detector for the scattering neutron spectrum is unknown. In this case, the shadow cone method cannot be used to measure neutron scattering [6].

To understand the impact of scattering on the neutron radiation field, neutron spectra for different operating space sizes were simulated using MCNP software. The operating space sizes were $4\times 4\times 4$, $6\times 6\times 6$, and $8\times 8\times 8$ m^3, respectively. The ideal neutron operating space was infinite. The neutron source was located in the center of the space, with an energy level of 14.1 MeV. The emission direction was isotropic. The number of simulated neutrons was 10^7. F5 and E5 statistical cards were used in the simulation. The F5 card was a point flux card, which was used to simulate neutron flux at the measurement point. The unit of measure is particles/cm^2. The E card established energy bin ranges, and the neutron spectrum at the measurement point was obtained from the combination of the F5 and E5 cards. The neutron fluxes in different energy regions were counted as 1 m away from the neutron source. The results are shown in Fig. 1.

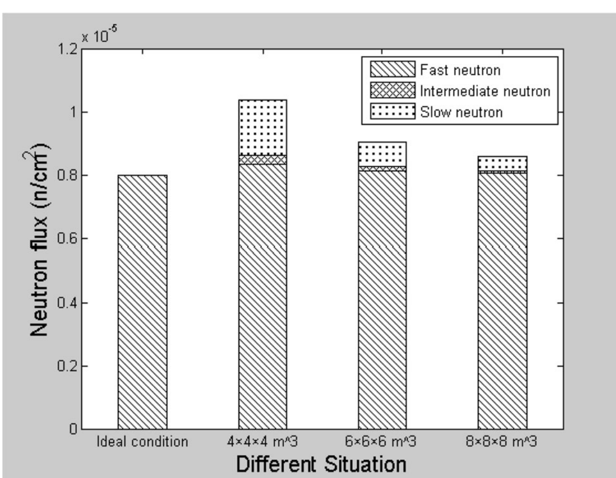

Fig. 1 Neutron fluxes for different energy regions under different conditions. *Note*: Fast neutron: $E>1$ MeV, Intermediate neutron: $0.001<E\leq 1$ MeV, Thermal neutron: $E\leq 0.001$ MeV

Under ideal conditions, the neutron energy in the radiation field was nearly the same as that of the neutron source with no scattering, whereas the neutron scattering became apparent in small operating spaces. Taking an operating space of $6\times 6\times 6$ m^3 as an example, the flux of intermediate and thermal neutrons accounted for 11.3% of the total neutron flux. To improve the monoenergetic property of neutrons, the scattering neutrons in the radiation field should be reduced.

2.2 Design idea

Neutrons have no charge, and no effective way to change their trajectories exists. Thus, a small-angle monoenergetic neutron source can be obtained only by absorbing surrounding neutrons with the use of a shielding collimator device [7]. The device has two functions. The first one is collimation [8], which involves moderating and absorbing neutrons outside the radiation field. Collimation constrains the neutron source within a small angle. The other function is shielding [9], which reduces the number of scattered neutrons and improves the monoenergetic property of neutrons.

Commonly used neutron shielding materials include boron-containing concrete, lead boron polyethylene, boron-containing stainless steel, and Al–B_4C alloy materials. However, these materials do not meet the requirements of neutron shielding. Lead boron polyethylene has good radiation shielding properties [10], but they have poor mechanical performance. Boron-containing stainless steel possesses high strength and good corrosion resistance [11]. However, boron has low solubility in stainless steel, thereby causing difficulty in the preparation of stainless steel with high boron content. Al–B_4C alloy possesses good thermal neutron absorption performance [12], and it can act as a structural material, but it involves a complex preparation process and a high production cost. Thus, shielding requirements cannot be met using only a single material. To absorb neutrons effectively, a multi-\layer shielding structure was used in this research [13].

The interactions of neutrons with matter involve short-range nuclear forces between neutron and atomic nuclei, and specific reaction types include elastic scattering, inelastic scattering, and radiation capture [14]. Fast neutrons interact with matter first by inelastic scattering, and heavy metal materials are usually selected as shielding materials because they have large [n, n], [n, n′], and [n, 2n] reaction cross sections, so that they can rapidly moderate fast neutrons to become intermediate neutrons below 1 MeV. The intermediate neutrons interact with matter by elastic scattering, and light materials that contain a high percentage of hydrogen offer a good choice. After being moderated by hydrogen materials, the energies of most intermediate neutrons are reduced to the thermal neutron energy region. The materials should have large thermal neutron reaction cross sections for absorption. During reactions between neutrons and matter, secondary γ rays will be generated, thereby allowing heavy metal materials to be added to the outermost layer to shield γ rays. The overall structure design idea is shown in Fig. 2.

3 Shielding collimator structure design

The shielding collimator device includes the collimator and the capture cave. Specifically, the collimator consists of multilayer moderated materials and is mainly used for producing a small-angle neutron source. The capture cave is mainly used for absorbing neutrons in the opposite direction of the radiation field, thus improving the monoenergetic property of neutrons in the radiation field.

3.1 Collimator structure simulation

3.1.1 Collimator aperture

The most common structures for an aperture are the cylindrical extraction structure, multi-tube extraction structure, and cone extraction structure [15]. These structures increase scattered neutrons outside the radiation field due to edge scattering. A multilayer, ladder-shaped aperture structure was adopted in this research, and a diagram of the structure is shown in Fig. 3.

Neutrons can be scattered at the edge of the aperture, which could increase the proportion of scattered neutrons outside the radiation field. The multilayer-shaped aperture forms a step shape according to the material of the collimator. Neutrons scatter at the edge of each ladder thereby greatly reducing the probability of neutrons directly hitting the outermost edge of the aperture and reducing the proportion of scattered neutrons outside the radiation field. The size of the collimator aperture is determined by the thickness of the shielding material and the angle of the neutron radiation field. The diameters of the radiation field under different cone angles are shown in Fig. 4.

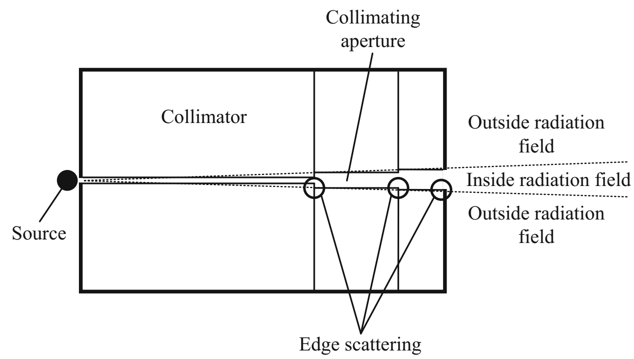

Fig. 3 Sketch of the neutron emission aperture

As shown in Fig. 4, when the neutron emission angle is 3°, the radiation field diameter is 5–20 cm for neutrons 1–4 m away from the neutron source, and the neutron intensity within the radiation field is 50–800 n cm^{-2} s^{-1} (a 10^8 s^{-1} neutron tube is adopted in this paper).

3.1.2 Collimator thickness

1. Heavy metal material

Heavy metal materials are used to moderate fast neutrons. The shielding properties of aluminum, iron, stainless steel, and boron carbide-containing aluminum were simulated [16]. The source was a 14.1 MeV isotropic neutron. The fast neutron (E>1 MeV) flux 1 m from the source was counted with the change in the thicknesses of materials. The results are shown in Fig. 5.

As shown in Fig. 5, iron and stainless steel produced better shielding properties for fast neutrons than aluminum and boron carbide-containing aluminum. Iron is a relatively

Fig. 2 Design idea for a shielding and collimating structure

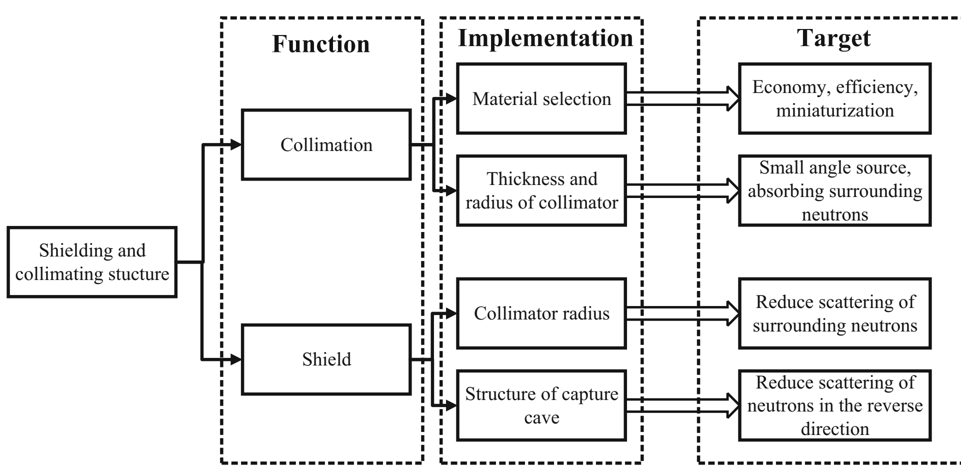

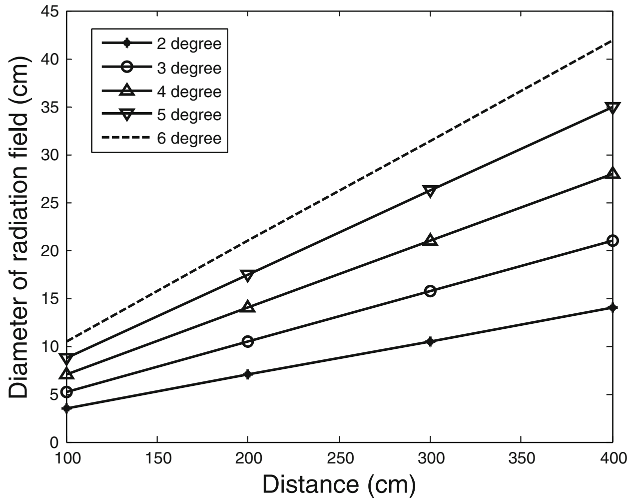

Fig. 4 Radiation field diameters at different distances

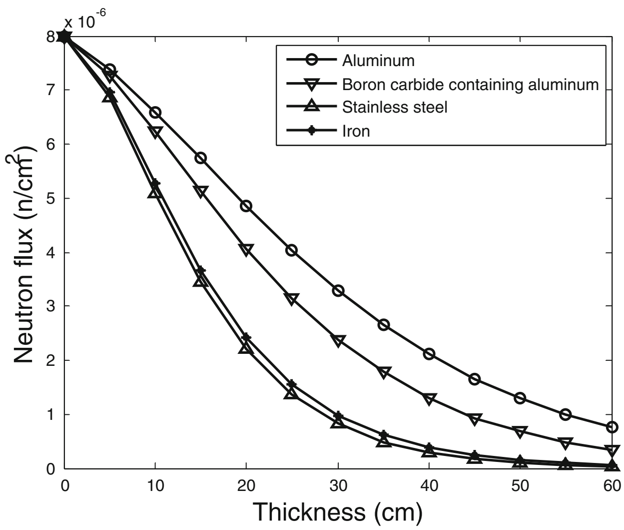

Fig. 5 Fast neutron flux with material thickness

common shielding material with a high density [17]. Iron releases more secondary γ rays under 10 MeV upon capturing thermal neutrons. Compared with iron, stainless steel has superior shielding properties for neutrons and γ performance, has a large inelastic scattering cross section, and can more effectively shield fast neutrons than iron. In addition, stainless steel has high structural integrity and a low price. Therefore, stainless steel is used for moderating fast neutrons.

Neutron fluxes in different energy regions for various thicknesses of stainless steel are shown in Fig. 6. The fast neutron flux decreased rapidly with an increase in the thickness of stainless steel; when the thickness of the stainless steel reached 50 cm, the fast neuron flux did not decrease significantly. Therefore, the thickness of the stainless steel was set to 50 cm.

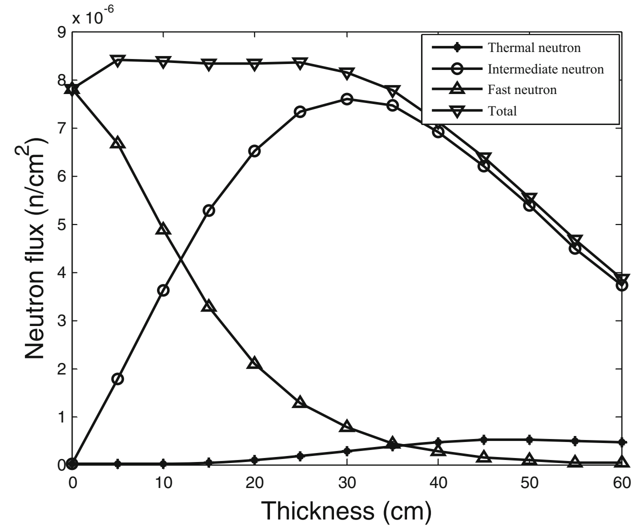

Fig. 6 Neutron fluxes for different energies and stainless steel layer thicknesses

2. Hydrogen-containing material

After moderation and adsorption by stainless steel, fast neutrons transformed into intermediate and thermal neutrons. Hydrogen-containing materials have large elastic scattering cross sections for intermediate neutrons [18]. B–10 can be used to absorb thermal neutrons. To simplify the structure and improve the moderating properties on neutrons, hydrogen-containing materials mixed with boron are usually adopted. These materials include borated polyethylene, boric paraffin, and boric acid. Boric acid aqueous solution, which is a simple and cheap protective material, must be placed in large containers made of a protective medium [19]. The mechanical processing property of boric paraffin is poor. Obtaining uniform boric paraffin is difficult [20, 21]. Therefore, borated polyethylene is selected for moderating intermediate neutron.

To test the moderating performance of polyethylene, the intermediate neutron that fluxes through different thicknesses of polyethylene was simulated. The neutron source was located in the stainless-steel-layer aperture port. The stainless steel layer was a hollow cylinder with an outer diameter of 100 cm, an inner diameter of 1.3 cm, and a thickness of 50 cm. The polyethylene behind the stainless steel layer had the same outer diameter as the stainless steel layer, but its inner diameter was determined by the thickness of the polyethylene. The intermediate neutron fluxes inside and outside the radiation field, which were 1 m away from the source with the change of the thicknesses of polyethylene, were counted. The results are shown in Fig. 7.

As shown in Fig. 7, with an increase in the thickness of polyethylene, the intermediate neutron fluxes inside and outside the radiation field decreased. When the

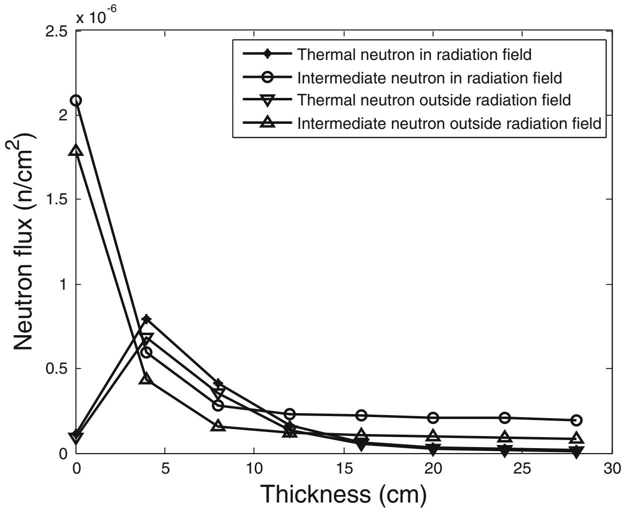

Fig. 7 Neutron flux with thickness of polyethylene

polyethylene thickness reached 20 cm, the intermediate neutron flux remained unchanged. Therefore, the thickness of the polyethylene was set to 20 cm.

To absorb the thermal neutrons, B–10 was added to the polyethylene material. The thermal neutron fluxes with different boron contents are shown in Fig. 8. When the boron content was 6%, the thermal neutrons were basically absorbed. The boron content of polyethylene was set to 6%.

3. Lead layer

When neutrons interacted with the matter, secondary gamma rays were generated. Lead was used to shield γ rays. The γ ray fluxes inside and outside the radiation field with different ranges of thicknesses were simulated. The neutron source and stainless steel layer had the same settings as those given above (Sect. 3.1.2). The thickness of borated polyethylene was 20 cm, and its inner diameter was 1.8 cm. The lead layer had the same outer diameter as the stainless steel and polyethylene. The inner diameter was determined by the thickness of lead. The γ ray fluxes 1 m away from the source were counted. The results are shown in Fig. 9.

As shown in Fig. 9, the fluxes inside and outside the radiation field of γ rays decreased with the increase in the thickness of lead. When the lead thickness was 2 cm, the γ ray flux in the radiation field reached a minimum level. When the thickness of lead reached 8 cm, the γ ray flux outside the radiation field did not decrease significantly. The γ rays were lower by two orders of magnitude than the rays with no lead shielding. Therefore, the thickness of the lead was set to 8 cm.

3.1.3 Collimator radius

Within the limited operating space, neutrons that pass through the collimator scatter on the wall, thus causing the neutrons to scatter in the radiation field. To reduce the interference of scattering, the radius of the neutron collimator was simulated. The neutron source was 14.1 MeV, being 1.5 m from the ground, and placed at the center of the collimation aperture. The front of the shielding was a three-layered collimation structure that was made of 50 cm of stainless steel, 20 cm of borated polyethylene, and 8 cm of lead. The inner diameter of each component measured 1.3, 1.8, and 2.0 cm, respectively. The rear part of the shield material was made of stainless steel, whose thickness was equal to the radius of the collimator. The entire device was placed in an operations room with dimensions of $6\times6\times6$ m^3, and the room's walls were 60-cm-thick concrete structures. The neutron fluxes inside and outside

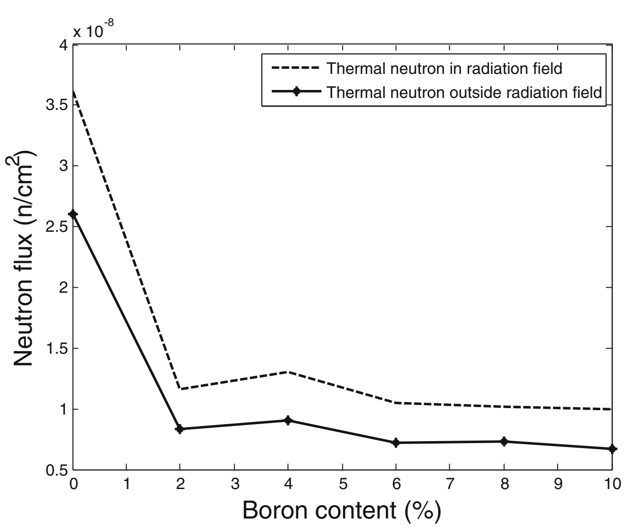

Fig. 8 Thermal neutron flux with boron content

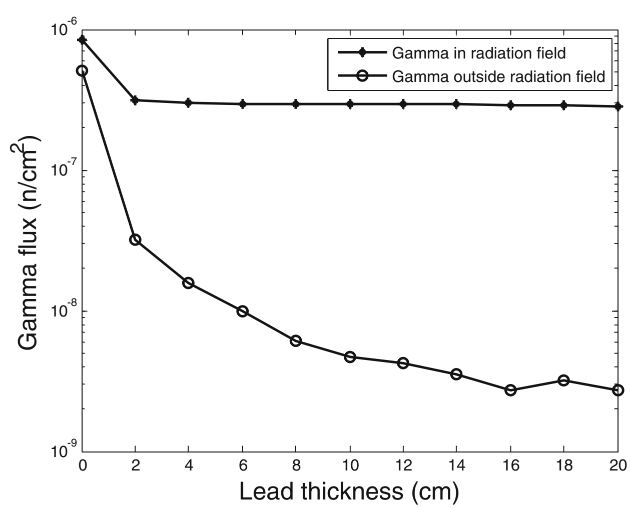

Fig. 9 γ ray flux with thickness of lead

the radiation field were counted. The results are shown in Fig. 10.

As shown in Fig. 10, as the collimator radius increased, the neutron flux decreased. When the radius of the collimator exceeded 30 cm, the neutron flux inside the radiation field changed slightly. When the radius of the collimator reached 35 cm, the neutron flux outside the radiation field was almost unchanged. Therefore, the radius of the collimator was set to 35 cm.

3.2 Capture cave structure simulation

The capture cave was cylindrical, made of stainless steel, and contained a cylindrical air layer. Figure 11 shows the basic structure of the capture cave.

The fast neutrons outside the capture cave were simulated. The collimator structure was set according to the simulation results in Sect. 3.1. The source was located in the cavity of the interface between the capture cave and the collimator, and its energy was 14.1 MeV. The fast neutron flux on the outside surface of the capture cave with the change in the thickness and diameter of the capture cave is shown in Fig. 12.

As shown in Fig. 12, fast neutron flux decreased with an increase in the thickness of the capture cave. When the thickness of the capture cave reached 25 cm, fast neutron flux outside the capture cave began to change slowly. Therefore, the thickness of the capture cave was set to 25 cm. However, the fluxes of thermal and intermediate neutrons outside the capture cave increased. To absorb the intermediate and thermal neutrons better, borated polyethylene was added to the outer surfaces of the capture cave and collimator. The proportions of intermediate and thermal neutrons in the radiation field with the change of thicknesses of borated polyethylene were simulated. The results are shown in Fig. 13.

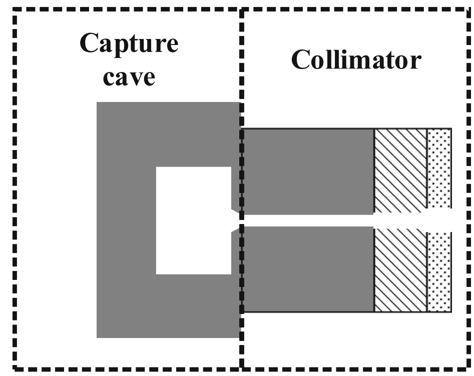

Fig. 11 Sketch of the capture cave and collimator

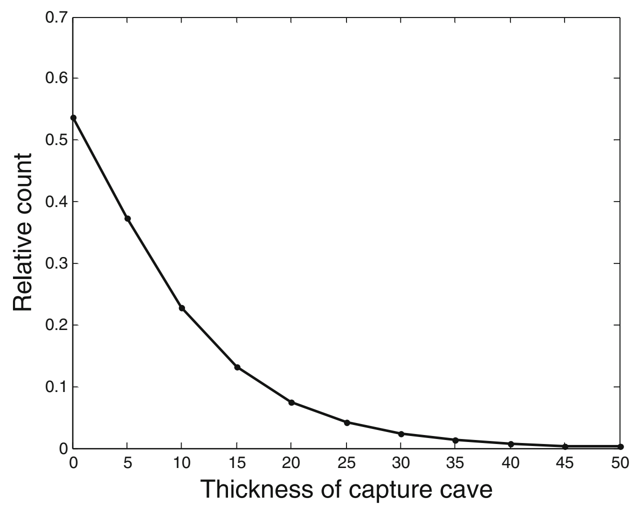

Fig. 12 Neutron flux with capture cave thickness

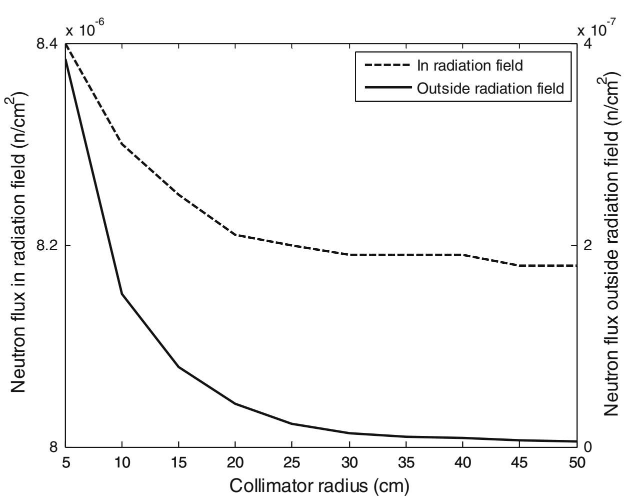

Fig. 10 Neutron flux with the collimator radius

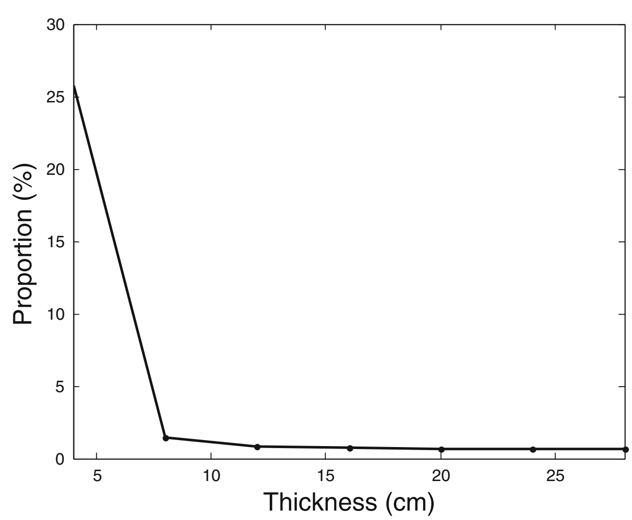

Fig. 13 Proportion of intermediate and thermal neutrons with the thickness of borated polyethylene

When the thickness of borated polyethylene increased to 12 cm, the proportion of intermediate and thermal neutrons in the total flux decreased to less than 1%. The thickness of the borated polyethylene outside the capture cave and collimator was set to 12 cm. The schematic and photograph of the shielding collimator device are shown in Fig. 14. A round hole with the same diameter as the neutron tube was opened at the joint between the collimator and the capture cave, and the neutron tube was placed along the hole so that the neutron exit position was at the center where the collimator and capture cave contacted.

4 Performance verification of shielding collimator structure

4.1 Neutron energy spectrum simulation

The shielding collimator device was placed in a $6 \times 6 \times 6$ m^3 space. D–D and D–T tubes were placed in the device. The neutron spectra 1 m from the radiation field were simulated. The results are shown in Fig. 15.

As shown in Fig. 15, after shielding and collimating, the energies of the neutrons were monoenergetic, and the dose rates of secondary γ rays 1 m from the radioactive source were 0.75 and 1.01 μGy h^{-1} for D–D and D–T tube, respectively.

4.2 Radiation field size simulation

The neutron fluxes 1 m from the neutron source at different sites on a plane vertical to the exit direction were simulated, and the results are shown in Fig. 16.

As shown in Fig. 16, the neutron source beam was limited within the range of 3°, and the neutron flux outside the radiation field was lower by two orders of magnitude than that within the radiation field 1 m away from the source.

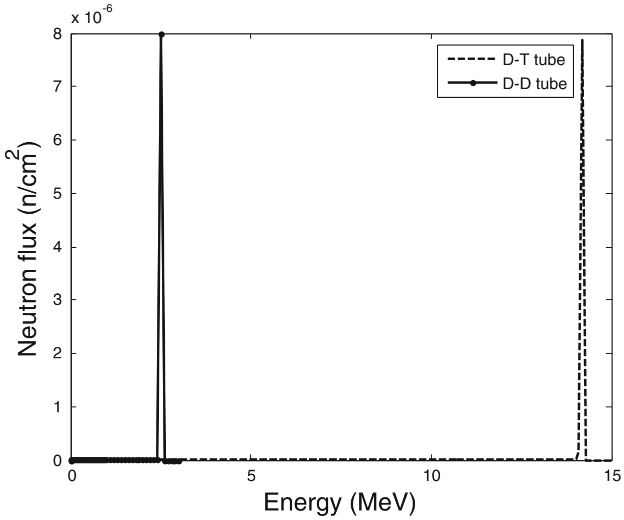

Fig. 15 Neutron spectra inside the radiation field

The simulation results showed that the shielding collimator device achieved the design goal.

4.3 Dose rate measurement

To test the shielding and collimating characteristics of the device, the neutron dose rates inside and outside the radiation field 2 m away from the source were measured in an experiment. The neutron source was the D–T tube, and the intensity of the source was 10^8. The detector used was a high-sensitivity regional neutron monitor produced by the Institute of High Energy Physics.

The background dose rate of the laboratory was 0.022 ± 0.018 μSv/h. The neutron dose rate inside the radiation field 2 m from the source was 1.75 ± 0.02 mSv/h, and the neutron dose rate outside the radiation field 2 m from the source was 18.56 ± 0.27 μSv/h. The simulation results of dose rates inside and outside the radiation field were 1.92 and 14.82 μSv/h, which were 9.7 and 20.1% of the errors with the experimental results, respectively. The simulation results were in the same order of magnitude as the

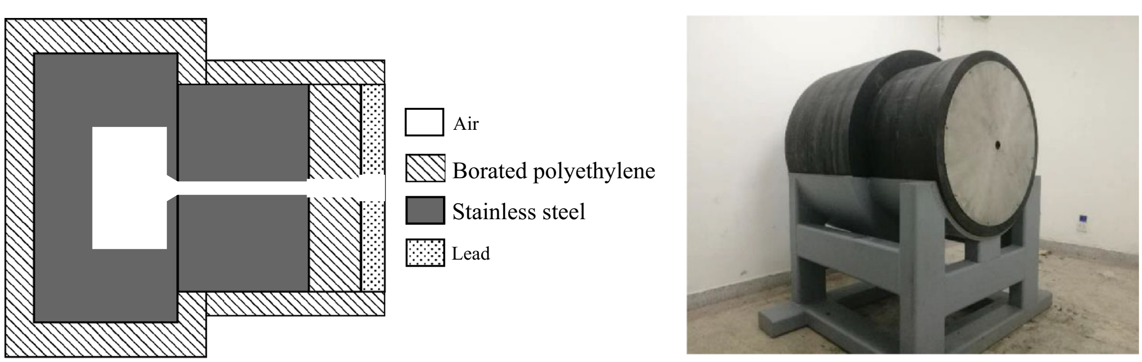

Fig. 14 Schematic and photograph of the shielding and collimating device

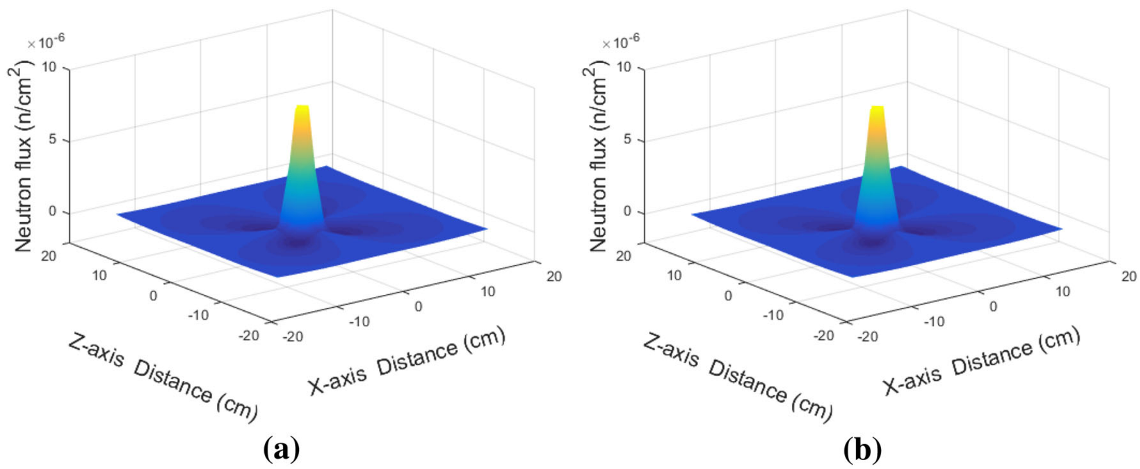

Fig. 16 (Color online) Examples of neutron fluxes represented in three dimensions. **a** D–T neutron flux, **b** D–D neutron flux

experimental results, and the errors may be the effect of the scattering of the supporting frame of the device. The dose rate value inside the radiation field was higher by two orders of magnitude than that outside the radiation field. The results illustrated the rationality of the structure of the device.

5 Conclusion

To obtain a small-angle monoenergetic neutron source, a shielding collimator device was designed for a 4π source of neutrons generated by small D–D and D–T neutron tubes. The device was divided into the collimator and the capture cave. The structure sizes of the collimator and the capture cave were simulated, and the device was built based on the simulation results. Thereafter, the performance of the device was verified by simulation and experiment. Results showed that the angle of the neutron source was controlled within a range of 3°, and the neutron flux outside the neutron irradiation field was lower by two orders of magnitude than those inside the radiation field, which was 1 m away from the source.

The designed device can generate a small-angle monoenergetic neutron source using D–D and D–T tubes. The neutron sources can find practical application in validating neutron dosimeters and in studying the characteristics of radiation resulting from the interactions of neutrons with matter.

References

1. M.K. Slifka, J.L. Whitton, Clinical implications of dysregulated cytokine production. J. Mol. Med. **78**, 74–80 (2000). https://doi.org/10.1007/s001090000086
2. G.W. Smith, L.G. Rice, Application of a 14 MeV neutron source to the detection of special nuclear material diversion. IEEE Trans. Nucl. Sci. **28**, 1637–1639 (1981). https://doi.org/10.1109/TNS.1981.4331486
3. X.H. Zheng, Y.B. Nie, X.C. Ruan et al., Experimental study of fast neutron radiography based on cockcroft-walton generator. At. Energy Sci. Technol. **49**, 1117–1121 (2015). https://doi.org/10.7538/yzk.2015.49.06.1117. **(in Chinese)**
4. S.T. Park, Neutron energy spectra of Cf, Am–Be source and of the D(d, n)He reaction. J. Radioanal. Nucl. Chem. **256**(1), 163–166 (2003). https://doi.org/10.1023/A:1023333016692
5. Y.H. Qiao, Progress in studies and applications of neutron tube. Nucl. Electron. Detect. Technol. **28**, 1134–1139 (2008). https://doi.org/10.3969/j.issn.0258-0934.2008.06.022
6. F.Q. Zhang, J.L. Yang, Z.H. Li et al., Monte Carlo simulation of effect of neutron scattering on image information in 14 MeV fast neutron radiography. Acta Phys. Sin. **56**, 3577–3583 (2007). https://doi.org/10.3321/j.issn:1000-3290.2007.06.089. **(in Chinese)**
7. C.X. Zhu, Y. Chen, Y.F. Mu et al., MCNP calculation of shielding performance for W–Cu shadow shield. At. Energy Sci. Technol. **40**, 21–25 (2006). https://doi.org/10.3969/j.issn.1000-6931.2006.01.005. **(in Chinese)**
8. X.H. Zhao, D.S. Gu, W.B. Ren et al., Study on the shielding material of 14 MeV neutrons collimation based on MCNP. J. Northeast Norm. Univ. **38**, 59–63 (2006). https://doi.org/10.3321/j.issn:1000-1832.2006.04.012. **(in Chinese)**
9. E.V. Every, A. Deyhim, Neutron scattering collimation wheel instrument for imaging research. J. Phys. **746**, 1 (2016). https://doi.org/10.1088/1742-6596/746/1/012023
10. T. Inatomi, T. Suzuki, H. Nakamura et al., U.S. Patent 8462910, 2013
11. C.X. Zhu, J.Q. Jiang, B.C. Lou, Measurements of DT neutron transmittance of Pb–B polythene. Nucl. Electronic. Detect. Tech. **29**, 988–992 (2009). https://doi.org/10.3969/j.issn.0258-0934.2009.05.015. **(in Chinese)**
12. X. Ding, X.L. Sun, Z. Li et al., Simulation of neutron reflecting and shielding property of various materials. Nucl. Technol. **40**, 7–11 (2017). https://doi.org/10.11889/j.0253-3219.2017.hjs.40.030201. **(in Chinese)**
13. P. Zhang, Z.W. Zhang, Optimal design of the carbon fiber reinforcing B4C/Al neutron absorbing materials. Nucl. Tech. **38**, 030605 (2015). https://doi.org/10.11889/j.0253-3219.2015.hjs.38.030605. **(in Chinese)**

14. K. Zhao, H.P. Guo, N. Lv et al., The design of "multiple energies from one source" in D–T neutron. Nucl. Sci. Technol. **27**, 107–112 (2016). https://doi.org/10.1007/s41365-016-0119-1
15. D.Z. Ding, *Neutron Physics* (Atomic Energy Press, Beijing, 2005)
16. Z. H. Wei, Dissertation. The Second Artillery Engineering University, 2013
17. K. Zhao, H.P. Guo, H.C. Wang et al., Design of shielding and filtering system for D–T neutron tube. At. Energy Sci. Technol. **48**, 768–772 (2014). https://doi.org/10.7538/yzk.2014.48.s0.0768. **(in Chinese)**
18. H.S. Hu, H. Xu, G.G. Zhang et al., Optimized design of shielding materials for nuclear radiation. At. Energy Sci. Technol. **39**, 363 (2005). https://doi.org/10.3969/j.issn.1000-6931.2005.04.018. **(in Chinese)**
19. W.S. Ji, J.W. Lee, S. Yu et al., Polyethylene/boron-containing composites for radiation shielding. Thermochim. Acta **585**, 5–9 (2014). https://doi.org/10.1016/j.tca.2014.03.039
20. D.R. Ochbelagh, H.M. Hakimabad, R.I. Najafabadi, Determination of neutron detectors shield used for the detection of landmines. Iran. J. Sci. Technol. Trans. A Sci. **32**, 227–233 (2008). https://doi.org/10.22099/ijsts.2008.2292
21. D.H. Zou, J.F. Du, Y.P. Yin et al., Development and performance verification of radiation screen door in fast critical assembly hall. J. Isotopes **28**, 98–106 (2015). https://doi.org/10.7538/tws.2015.28.02.0098